BRAIN
ORIGINAL ARTICLE

Bi-allelic variants of FILIP1 cause congenital myopathy, dysmorphism and neurological defects

Andreas Roos,[1,2,3,†] Peter F. M. van der Ven,[4,†] Hadil Alrohaif,[5,6] Heike Kölbel,[1] Lorena Heil,[4] Adela Della Marina,[1] Joachim Weis,[7] Marvin Aßent,[4] Stefanie Beck-Wödl,[8] Rita Barresi,[9] Ana Töpf,[5] Kaela O'Connor,[2] Albert Sickmann,[10] Nicolai Kohlschmidt,[11] Magdeldin El Gizouli,[12] Nancy Meyer,[1] Nassam Daya,[3] Valentina Grande,[4] Karin Bois,[4] Frank J. Kaiser,[12] Matthias Vorgerd,[3] Christopher Schröder,[12] Ulrike Schara-Schmidt,[1] Andrea Gangfuss,[1] Teresinha Evangelista,[5,13] Luisa Röbisch,[10] Andreas Hentschel,[10] Anika Grüneboom,[10] Dieter O. Fuerst,[4] Alma Kuechler,[12] Andreas Tzschach,[14,†] Christel Depienne[12,†] and Hanns Lochmüller[2,15,†]

[†]These authors contributed equally to this work.

Filamin-A-interacting protein 1 (FILIP1) is a structural protein that is involved in neuronal and muscle function and integrity and interacts with FLNa and FLNc. Pathogenic variants in filamin-encoding genes have been linked to neurological disorders (*FLNA*) and muscle diseases characterized by myofibrillar perturbations (*FLNC*), but human diseases associated with *FILIP1* variants have not yet been described. Here, we report on five patients from four unrelated consanguineous families with homozygous *FILIP1* variants (two nonsense and two missense).

Functional studies indicated altered stability of the FILIP1 protein carrying the p.[Pro1133Leu] variant. Patients exhibit a broad spectrum of neurological symptoms including brain malformations, neurodevelopmental delay, muscle weakness and pathology and dysmorphic features. Electron and immunofluorescence microscopy on the muscle biopsy derived from the patient harbouring the homozygous p.[Pro1133Leu] missense variant revealed core-like zones of myofibrillar disintegration, autophagic vacuoles and accumulation of FLNc. Proteomic studies on the fibroblasts derived from the same patient showed dysregulation of a variety of proteins including FLNc and alpha-B-crystallin, a finding (confirmed by immunofluorescence) which is in line with the manifestation of symptoms associated with the syndromic phenotype of FILIP1opathy.

The combined findings of this study show that the loss of functional FILIP1 leads to a recessive disorder characterized by neurological and muscular manifestations as well as dysmorphic features accompanied by perturbed proteostasis and myopathology.

1 Department of Pediatric Neurology, Center for Neuromuscular Disorders, Center for Translational Neuro- and Behavioral Sciences, University Duisburg-Essen, 45147 Essen, Germany
2 Brain and Mind Research Institute, Children's Hospital of Eastern Ontario Research Institute, Ottawa, ON, K1H 8L1, Canada
3 Department of Neurology, University Hospital Bergmannsheil, Heimer Institute for Muscle Research, 44789 Bochum, Germany
4 Department of Molecular Cell Biology, Institute for Cell Biology, University of Bonn, 53121 Bonn, Germany

Received October 03, 2022. Revised March 16, 2023. Accepted April 11, 2023. Advance access publication May 10, 2023

5 John Walton Muscular Dystrophy Research Centre, Translational and Clinical Research Institute, Newcastle University and Newcastle Hospitals NHS Foundation Trust, Newcastle upon Tyne, NE1 3BZ, UK
6 Kuwait Medical Genetics Center, Sabah Hospital, Kuwait City, Kuwait
7 Institute of Neuropathology, RWTH Aachen University Hospital, 52074 Aachen, Germany
8 Institute of Medical Genetics and Applied Genomics, University of Tübingen, 72076 Tübingen, Germany
9 San Camillo IRCCS, 30126 Venezia - Lido, Italy
10 Department of Bioanalytics, Leibniz-Institut für Analytische Wissenschaften - ISAS - e.V., 44227 Dortmund, Germany
11 Institute of Clinical Genetics and Tumour Genetics, 53111 Bonn, Germany
12 Institute of Human Genetics, University Hospital Essen, University of Duisburg-Essen, 45147 Essen, Germany
13 Nord/Est/Ile-de-France Neuromuscular Reference Center, Institute of Myology, Pitié-Salpêtrière Hospital, APHP, Sorbonne University, 75013 Paris, France
14 Medical Center, Faculty of Medicine, Institute of Human Genetics, University of Freiburg, 79106 Freiburg, Germany
15 Division of Neurology, Department of Medicine, The Ottawa Hospital, Ottawa, ON, K1H 8L1, Canada

Correspondence to: PD Dr Andreas Roos
University Medicine Essen, Department of Pediatric Neurology
Hufelandstrasse 55, 45147 Essen, Germany and University Hospital Bergmannsheil
Heimer Institute for Muscle Research
Bürkle de la Camp-Platz 1, 44789 Bochum, Germany
E-mail: roos@andreas-roos.de

Keywords: MFM/myofibrillar myopathy; vacuolar myopathy; protein aggregate myopathy; FLNC; FLNA

Introduction

Neurological diseases including neuromuscular disorders are frequently caused by genetic variants affecting structural proteins crucial for muscle cell contraction as well as neuronal function and maintenance.[1]

Filamin-A-interacting protein 1 (FILIP1) is a structural protein known to regulate cell polarity and motility in neocortical subventricular and intermediate zones during radial migration indicating a crucial role in neuronal function.[2] Pathogenic variants in the X-chromosomal gene *FLNA* encoding its major binding partner FLNa lead to a spectrum of neurological manifestations depending on the sex of the affected individual. These include brain malformations such as periventricular heterotopia in addition to cardiovascular abnormalities, skeletal dysplasia and facial dysmorphisms.[3] FILIP1 is even more highly expressed in skeletal muscle[4] and knockdown of *Filip1* was shown to inhibit myogenic differentiation of murine muscle cells.[5] Recently, combined proximity proteomics and interaction studies also identified FILIP1 as a direct binding partner of FLNc, the main filamin expressed in striated muscle. Of note, FILIP1 binding induces filamin degradation, thereby negatively regulating its function.[6] Interestingly, dual-site phosphorylation of FLNc reduces FILIP1 binding, providing a mechanism to shield FLNc from FILIP1-mediated degradation and enabling fast dynamics of myofibrillar Z-disc-associated FLNc.[6] A large number of dominant variants and one recessive variant in *FLNC* have already been linked to human myopathies and cardiomyopathies.[1,7,8] Thus, although pathogenic variants in both FILIP1-binding partners are linked to the manifestation of neurological diseases which in the case of *FLNA* might be associated with additional clinical features such as facial dysmorphism, no disease has thus far been linked to variants in the *FILIP1* gene.

Here, we report five patients from four unrelated families with bi-allelic pathogenic variants in *FILIP1*. The patients presented with neurodevelopmental phenotypes including intellectual disability as well as facial dysmorphism, myopathy and brain malformations in two patients. Combined histological, functional and proteomic studies reveal a FILIP1-related dysregulation of several proteins including FLNc and altered solubility and stability of missense-mutant FILIP1, indicating the pathogenicity of the investigated FILIP1 variants. These results, in combination with findings from ultrastructural investigations revealing myofibrillar disintegration and focal aggregation of proteins that are typical for myofibrillar myopathy (MFM)-associated aggregates, introduce *FILIP1* as a novel gene for neurological and neuromuscular manifestations accompanied by facial dysmorphisms.

Materials and methods

DNA studies

DNA samples from proband Patients 1–3 and their parents were subjected to whole exome sequencing. Libraries were created with an Illumina exome capture (38 Mb target) kit and sequenced with a mean target coverage of 80× (Genomics Platform, Broad Institute of MIT and Harvard, Cambridge, USA). Data analysis was carried out in two stages, first searching for pathogenic/likely pathogenic variants in genes known to be associated with the clinical presentation (*in silico* panel). If no variants were identified, and given the known consanguinity in the family, the full exome was interrogated by applying a stringent search for highly damaging homozygous variants such as nonsense, splice region and frameshift variants absent in the control population (gnomAD; http://gnomad.broadinstitute.org).

The exome of Patient 4 and his parents was sequenced at the Brain Paris Institute facility (ICM, Paris, France). Libraries were prepared using the SeqCap® EZ Human Exome Probes v3.0 (Roche) and sequenced by paired-end 150 bp massively parallel sequencing on a NextSeq500 sequencer (Illumina), according to the manufacturers' instructions. Reads were mapped on the hg38 reference genome using varlociraptor.[9] Variant filtering was based on the following criteria: allele frequency below 0.1% in the control population (gnomAD v2.1), variants altering the coding sequence or splice sites of a coding gene, and inheritance compatible with an isolated or recessive condition such as *de novo* heterozygous, homozygous, hemizygous or compound heterozygous variants.

Exome sequencing of Patient 5 was conducted on genomic DNA. Coding genomic regions were enriched using a SureSelect XT Human All Exon Kit V7 (Agilent Technologies) for subsequent sequencing as 2 × 100 bp paired-end reads on a NovaSeq6000 system (Illumina). Generated sequences were analysed using the megSAP pipeline (https://github.com/imgag/megSAP). Clinical variant prioritization included different filtering steps [e.g. minimum allele frequency (MAF) < 0.1% in 1000 G, ExAC or gnomAD, in-house database] and was conducted independently by two trained diagnostic molecular geneticists according to an in-house standard operating procedure.[10]

FILIP1 variants were confirmed and segregated in available family members by Sanger sequencing. AlamutVisual 2.15 (Interactive Biosoftwares) and Combined Annotation Dependent Depletion (CADD) scores[11] were used to interpret variants (conservation of amino acid, *in silico* predictions). *FILIP1* variants are annotated based on NM_015687.5, the 1213 amino acid long Matched Annotation from NCBI and EMBL-EBI (MANE) isoform of *FILIP1*.[12] Two other FILIP1 isoforms, NM_001289987.3 [1216 amino acids (aa)] and NM_001300866.3 (1177 aa), exist.

Histology and electron microscopy

Serial cryosections (10 μm) of transversely oriented muscle blocks were stained following standard procedures with haematoxylin and eosin (H&E), as well as nicotinamide adenine dinucleotide tetrazolium reductase (NADH-TR). Light microscopic investigations were performed using a Zeiss Axioplan epifluorescence microscope equipped with a Zeiss Axio Cam ICc 1. Glutaraldehyde-fixed muscle biopsy specimens from Patient 3 were processed for ultrastructural examination by standard procedures. The tissue was post-fixed in 1% osmium tetroxide and embedded in Epon 812. Semithin sections for light microscopy were stained with toluidine blue. Ultrathin sections were contrasted with uranyl acetate and lead citrate and examined using a Philips CM10 transmission electron microscope as described previously.[13]

Immunostaining of muscle cryosections

For immunofluorescence studies, 10 μm cryosections were air dried and fixed in acetone at −20°C for 10 min. After air-drying, the sections were blocked using 10% NGS, 1% BSA in PBS for 1 h at room temperature. Subsequently, sections were incubated for 1 h with a mixture of two primary antibodies diluted in 3% NGS, 1% BSA in PBS. Applied antibodies were a combination of RR90 anti-FLNc (1:50; mouse IgA)[14] with either a rabbit antiserum recognizing Xin/XIRP1 and XIRP2 (1:1000)[15] or anti-desmin mouse monoclonal antibody DE-R-11 (1:100; mouse IgG1, Leica/Novocastra), or a rabbit antiserum specific for FILIP1 (1:150; HPA053564, Atlas antibodies). For some samples, tissue sections were stained with RR90, anti-FILIP1 and monoclonal antibody XC4 that recognizes Xin isoform A (1:2)[16] or monoclonal antibody MHCn (1:10; mouse IgG1, Leica/Novocastra) that recognizes neonatal myosin. After extensive washing with PBST (PBS containing 0.05% Tween), sections were incubated with the appropriate combination of goat anti-mouse IgA Alexa 488 (Southern Biotech), goat anti-mouse IgG1 Alexa 594 (Jackson ImmunoResearch), goat anti-rabbit Alexa 594 plus (ThermoFisher Scientific) and/or goat anti-rabbit Alexa 647 (ThermoFisher Scientific) or for 1 h. After extensive washing with PBS and a short wash in water, sections were mounted with FluoromountG mounting medium. Sections were observed and photographed using an AxioImager M1 microscope (Carl Zeiss). Zen 2.6 software (Carl Zeiss) was used for image processing.

Recombinant protein expression and analysis

The cDNA of *FILIP1* encoding the amino acids 189-785 (FILIP1-coil) and 776-1177 (FILIP1-CT) of isoform UniProt Q7Z7B0-2 was cloned in the bacterial expression vector pET23-EEF[17] enabling the expression of the recombinant proteins with a carboxyterminal His6-EEF tag. Induction of protein synthesis and purification of the recombinant proteins was performed as described. In brief, bacteria were lysed in lysis buffer and sonified. The insoluble fraction was removed by centrifugation (20 min, 3000*g*) and soluble proteins in the supernatant were purified using Ni^{2+}-NTA agarose beads and used for further experiments. The relative amount of recombinant protein in the soluble and insoluble fractions were analysed by SDS-PAGE. Susceptibility of mutant and wild-type FILIP1-coil and FILIP1-CT to proteolytic digestion by thermolysin and/or trypsin was analysed as described before.[7] The purified FILIP1-coil proteins were tested for their ability to di- or oligomerize by cross-linking assays. Purified proteins were dialyzed against CL-Buffer (600 mM NaCl, 1 mM $MgCl_2$, 1 mM DTT, pH 7.4). To 50 μl of 10–20 μM protein solution, 1 μl 30–65 mM EGS in DMSO was added, and the mixture was incubated at 37°C. After different incubation periods, 5 μl of the reaction mixture was removed, and the reaction was stopped by addition of 2 μl 5× SDS sample buffer. Samples were heated for 5–10 min at 95°C and analysed by western blotting using the antibody YL1/2, which recognizes the EEF-tag of the recombinant proteins, and a horseradish peroxidase-conjugated goat anti-rat Ig secondary antibody (Jackson ImmunoResearch). Integrated intensities of polyacrylamide gels and western blots were quantified using a ChemiDoc MP Imaging System and Image Lab software (Version 6.1.0; Bio-Rad Laboratories, Feldkirchen, Germany). All statistical analyses were performed using GraphPad Prism and paired *t*-test.

Fibroblast culture and subsequent *in vitro* studies

Fibroblasts derived from controls, Patient 3 and one male *FLNC*-patient (c.4984C>T; p.[Gln1662Ter]) were cultured as described previously.[18] For proteomic profiling, cells were collected by scraping-down, washed twice with ice-cold PBS, snap-frozen in liquid nitrogen and stored in −80°C until further processing. For proteomic profiling, functional and immunofluorescence studies, fibroblasts derived from three male healthy donors (controls) were included.

Analysis of *FILIP1* gene expression

Total RNA was isolated from fibroblasts of Patient 3 and one control using the High Pure RNA Isolation Kit (Roche), and cDNA was prepared using FireScript reverse transcriptase (Solis BioDyne) and random nonamers according to the instructions of the manufacturers. cDNA was amplified by PCR using FIREPol Master Mix Ready to Load (Solis BioDyne) with oligonucleotides specific for all isoforms of *FILIP1* (CCAGGAATCACCTCTCCTCA and TGGTCAGAT TTCCTGCTCCT) and for *GAPDH* (AGGTCGGAGTCAACGGATTTG and TGTAAACCATGTAGTTGAGGTCA) as control. Samples were loaded on a 2% agarose gel, and the gel was photographed using a Gel Doc Gel Documentation System (Bio-Rad). Given that the variation c.3398C>T deletes a BshTI restriction site, amplicons were purified and digested with this enzyme to confirm the homozygous expression of the mutant variant in our Patient 3.

Proteomic profiling

Previous studies have shown that proteinogenic profiling on cultured skin fibroblasts enables the study of the molecular aetiology

of rare neurological diseases.[19] Here, fibroblasts derived from Patient 3 and sex- and age-matched controls ($n = 3$) were cultured from skin biopsies and collected for proteomic profiling as described previously.[19] Three technical replicates of patient fibroblasts and two technical replicates of each of the three controls were included in the experiment. A detailed description is provided in the Supplementary material.

Microscopic studies

Control, *FLNC*- and *FILIP1*-mutant fibroblasts cultivated on coverslips were fixed with 4% PFA for 15 min at room temperature. Coverslips were blocked for 1 h at room temperature with blocking buffer (1% BSA/0.1% Tween20/0.1% DMSO/PBS). Samples were then incubated for 1 h at room temperature with either rabbit anti-human FLNc (1:50), rabbit anti-human FLNa (1:400), rabbit anti-human FILIP1 (1:100), or rabbit anti-human alpha-B-crystallin (1:400). Unbound primary antibodies were removed by washing three times with washing buffer (0.1% Tween20/0.1% DMSO/PBS). Secondary staining was performed for 1 h each at room temperature with anti-rabbit Alexa Fluor 555 plus (1:100) and DAPI (1:500). Unbound antibodies and dyes were removed by washing three times with washing buffer and samples were mounted with DAKO fluorescent mounting medium.

High-resolution scans of fibroblasts were performed using a Leica TCS SP8 confocal laser scanning microscope with acousto-optic tunable filters, an acousto-optic beam splitter, internal hybrid detectors (HyD SP) and a high-precision LMT200 scanning stage. Imaging of samples embedded in coverslips was performed using a Leica HC PL APO 63×/1.20 W CORR objective in combination with variable digital zoom factors depending on fibroblast size. In the first sequential scan, FLNc, FLNa, FILIP1 and alpha-B-crystallin, each labelled with Alexa Fluor 555 plus, were excited with an argon laser at 561 nm and detected with a HYD detector at 600–650 nm. In a second sequence, actin fibres labelled with phalloidin-Alexa Fluor 647 were excited with a HE-Ne laser at 633 nm and detected with an internal HyD at 650–700 nm. In the last sequence, DAPI was excited with a diode-pumped solid-state laser at 405 nm and detected with an internal HyD at 450–500 nm. The generated images were deconvoluted using Huygens Professional (SVI) and reconstructed using Imaris software (Bitplane). To generate the circular colour map and coherence orientation index (COI), the confocal scanned z-stacks were loaded into ImageJ and converted to maximum intensity projections (MIP) using the Z project tool. Individual cells were identified by manually defining the region of interest (ROI) and visually separated by clearing the area outside the ROI. Isolated cells were then aligned horizontally, colour maps were generated and the COI of each cell was determined using the OrientationJ plugin. The filopodia of human fibroblasts were manually isolated optically from the rest of the actin fibre skeleton of the cell based on their morphological characteristics and quantified. Filopodia length and branching were quantified using the ImageJ plugin 'Analyze Skeleton (2D/3D)'.[20] Statistical analysis of COI values was performed using GraphPad Prism 9.

Actin fibre staining with FITC-Phalloidin (Alexa Fluor 488; ab235137, Abcam) was performed according to the manufacturer's instructions in human fibroblasts and imaging was carried out using a Zeiss Axio Observer.Z1 microscope with Apotome to address the effect of cytochalasin-D treatment (see the next section). In addition, the effect of cytochalasin-D exposure on cellular morphology was monitored by light microscopy.

MTT assay

To further address the effect of pathogenic variants in *FLNC* and *FILIP1*, on cytoskeletal integrity, cellular viability was monitored by measuring the metabolic activity of fibroblasts by means of an MTT assay (a colorimetric assay; 3-[4,5-dimethylthiazol-2-yl]-2,5 diphenyl tetrazolium bromide) under basal conditions (non-treated) and after 90 min treatment with 0.05 µg/ml µM cytochalasin-D (ThermoFisher; PHZ1063), a cell-permeable inhibitor that binds actin filaments. The MTT assay was carried out as described previously.[21] In addition to the patient-derived cells, fibroblasts of three different healthy donors serving as non-disease controls were included and data of these controls were merged.

In silico studies of FILIP1 missense variants

FILIP1 contains a large region that is predicted to form coiled coils,[22] but an experimentally defined protein structure for FILIP1 is not available through Protein Data Bank. Therefore, we used computational modelling to predict the 3D structure and the associated alterations that occur due to missense variants found in patients. For that purpose, AlphaFold2, the modelling system found to be the most accurate in the CASP14 (Critical Assessment of Structure Prediction) competition, was used to generate the predicted structure for wild-type FILIP1.[23] This structure was subsequently used with PremPS (Predicting the Effects of Mutations on Protein Stability) to predict changes to the protein structure caused by amino acid substitutions identified in two patients, p.[Arg386Cys] and p.[Pro1133Leu], on FILIP1. PremPS has been shown to more successfully predict changes in stability from single mutations than its competitors.[24] The desired variants were manually selected, and PremPS calculated the predicted unfolding Gibbs free energy change [DDG (kcal/mol)] and changes to non-covalent interactions. The images were generated directly through PremPS. Additionally, a prediction of coiled coil formation and the effect of the p.[Arg386Cys] variant was analysed using the COILS Server at embnet.vital-it.ch.

Results

Clinical findings

Clinical data are presented in Fig. 1 and summarized in Table 1. A detailed description of each case is also provided in the Supplementary material.

In all patients, clinical manifestations were present from birth, mainly as floppy infants with hypotonia (4/5). The main symptoms in childhood included delayed motor milestones (5/5), delayed speech development (4/4), intellectual disability (4/4), distinct contractures (3/5), clubfeet (2/5) and microcephaly (2/5). As Patient 4 died at the age of 13 months, the presence of intellectual disability and perturbed speech development could not be evaluated; however, parents and neuropaediatric specialists observed a marked reduction of infant language production. Brain malformations were identified in two patients and included occipital encephalocele, semilobar holoprosencephaly, atretic cephalocele, malformation of tentorium and absent rostrum (Fig. 1 and Table 1). One patient (Patient 4) was affected by epilepsy with generalized and focal tonic-clonic seizures as well as myoclonic seizures from the age of 5 months. His epilepsy was stable under therapy with levetiracetam and phenobarbital; however, he died at the age of 13 months as a result of an infection. Moreover, dysmorphisms shared by the patients as a recognizable 'Gestalt' include epicanthus, down-slanted

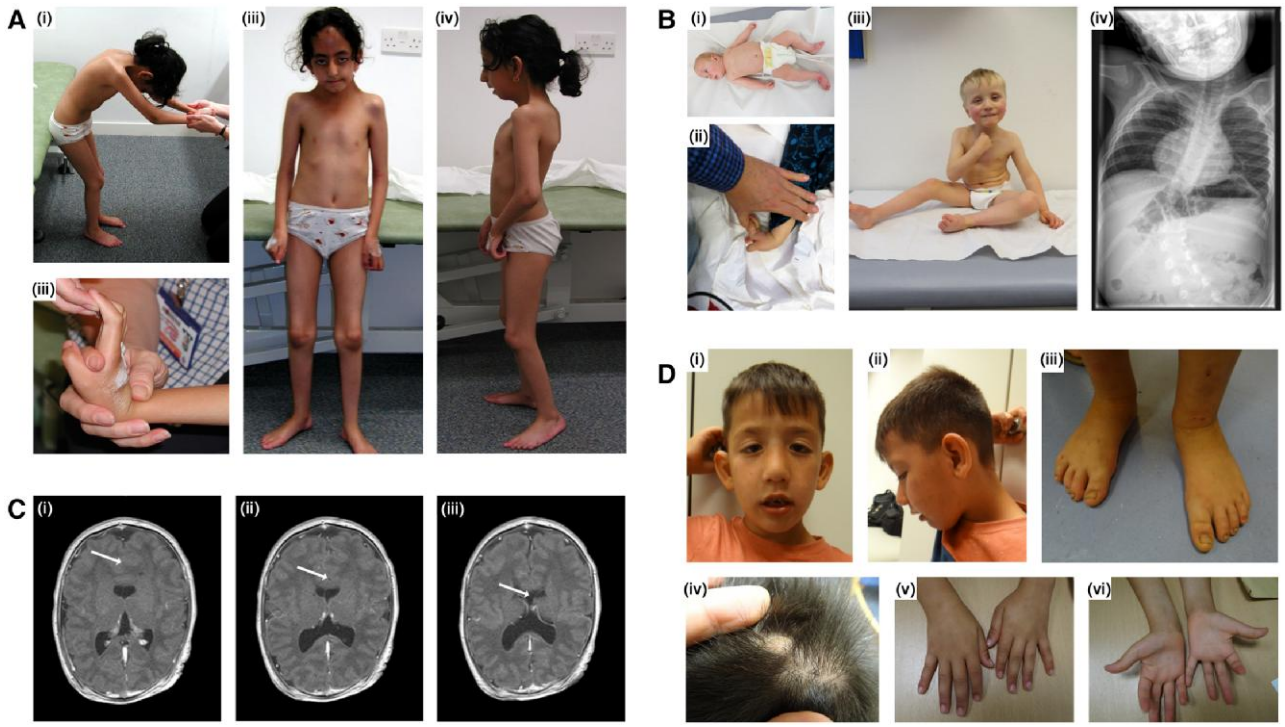

Figure 1 Presentation of disease features found in our cohort *FILIP1*-patients defining the congenital syndrome. (**A**) Female Patient 1 from Family A with homozygous p.[Arg57*] FILIP1 variants. Clinical findings include neck webbing, rigid spine, kyphoscoliosis, elbow and knee flexion contractures and bilateral foot pronation as well as flexion contractures of the fingers (**i–iv**). Dysmorphic features include large forehead with prominent ridging of the metopic suture, large prominent ears, prominent nose and micrognathia, ptosis, myopathic face (**iii** and **iv**). Photographs were taken at the age of 9 years. (**B**) Male index patient from Family B with homozygous p.[Pro1133Leu] FILIP1 variants. **B(i)** shows the patient as a floppy baby with congenital clubfeet and adducted thumbs and joint hyperlaxity is shown in **ii**. **B(iii)** shows the patient as a toddler (able to sit without support) presenting with ptosis, epicanthus, down-slanted palpebral fissures, hypertelorism, broad root of the nose/depressed nasal bridge. **B(iv)** shows severe scoliosis found in this patient. Photographs/images were taken at the age of 4 months (**i**), 2.5 years (**ii**) and 3.5 years (**iii** and **iv**). (**C**) shows a lobar holoprosencephaly with agenesis of corpus callosum (indicated by arrows) in Patient 4 from Family C. MRI was carried out at the age of 14 days. (**C**) shows Patient 5 from Family D presenting with protruding ears, ptosis, epicanthus, down-slanted palpebral fissures, hypertelorism, broad root of the nose/depressed nasal bridge (**i** and **ii**). Foot abnormalities are not present (**iii**). **D(iv)** shows residual material of an occipital encephalocele. **D(v** and **vi)** show single transverse palmar crease on the left hand, but otherwise absence of major anomalies. Photographs were taken at the age of 5 years and 9 months.

palpebral fissures, hypertelorism, broad root of the nose/depressed nasal bridge and high arched palate (Fig. 1). Dysmorphic features only observed in single patients include ptosis, small hypoplastic deep-set nails, accessory nipple (left), simian crease of the left hand, tapering fingers and broad great toes. Recurrent respiratory infections occurred in two patients and cardiac abnormalities (Atrial septal defect type II, Ventricular septal defect) were present in one patient.

Molecular genetic findings

Through exome sequencing analysis, homozygous *FILIP1* variants were identified in these five patients (three males and two females) from four consanguineous families (Table 1 and Fig. 2A). Genetic results related to *FILIP1* are summarized in Supplementary Table 2 and variants identified in additional genes (none of them likely to be causative of the clinical manifestation in our patients) are summarized in Supplementary Table 3. Stop-gain variants were identified in two affected siblings (Patients 1 and 2; NM_015687.5:c.169C>T; p.[Arg57*]) and in Patient 4 (NM_015687.5:c.115C>T; p.[Arg384*]), while missense changes were identified in Patient 5 (NM_015687.5:c.1156C>T; p.[Arg386Cys]) and Patient 3 (NM_015687.5:c.3398C>T; p.[Pro1133Leu]) (Fig. 2B and C). The variant in Patient 5 is located in the predicted extended coiled coil region of FILIP1, whereas the variant in Patient 3 is localized in a motif (KVTSTITITP) with unknown function. This motif resides in the part of FILIP1 that binds filamins and that is highly conserved between FILIP1 and FILIP1L (Fig. 2D). Sequence alignment of the region flanking the substituted amino acids in Patients 3 and 5 (i.e. Arg386 and Pro1133) shows that these residues are highly conserved amongst species up to zebrafish, but also between FILIP1 and the paralogous protein FILIP1L (Fig. 2D).

All variants had CADD scores above 24 and were absent or present at very low allele frequencies in the control population (gnomAD v2.1), and never detected in the homozygous state (Supplementary Table 3).

Muscle biopsy findings

H&E staining of cryosections of muscle biopsies derived from Patients 1 and 3 revealed an overall very mild pathology with only a few fibre-size variations at the histological level [Fig. 3A(i and ii)]. NADH-TR reaction did not show prominent alterations [Fig. 3A (i and iv)].

Electron microscopy studies performed on a quadriceps biopsy of Patient 3 revealed numerous small core-like zones of myofibrillar disintegration [Fig. 3B(i–iii)] in addition to small subsarcolemmal accumulation of material composed of fine, mildly osmiophilic granules [Fig. 3B(iv and v)]. Occasionally, subsarcolemmally

Table 1 Clinical findings in neuropaediatric patients with homozygous *FILIP1* variants

	Family A		Family B	Family C	Family D
	Patient 1	Patient 2	Patient 3	Patient 4	Patient 5
FILIP1 variant	c.169C>T; p.[Arg57*] hmz	c.169C>T; p.[Arg57*] hmz	c.3398C>T; p.[Pro1133Leu] hmz	c.115C>T; p.[Arg384*] hmz	c.1156C>T; p.[Arg386Cys] hmz
Gender	Female	Female	Male	Male	Male
Consanguinity	Yes	Yes	Yes	Yes	Yes
Origin	Pakistan	Pakistan	Germany	Turkey	Syria
Onset	Congenital	Congenital	Congenital	Congenital	Congenital
First symptoms	Floppy infant, contractures	Floppy infant, contractures	Floppy infant, clubfeet	Floppy infant, contractures of hands, clubfeet, bilateral cleft lip and palate	Occipital encephalocele
Motor milestones	Delayed (sitting without support at 18 mo)	Delayed	Delayed (sitting without support at 42 mo)	Not achieved (last exam. at age 13 mo)	Delayed (walking at 3 y)
Speech development	Delayed (first words 2.5 y)	Delayed (first words 2.5 y)	Delayed (first words at 3 y)	No	Delayed (first words at 4 y)
Intellectual disability/learning difficulties	Yes	Yes	Yes	Yes (no development)	Yes
Joint hypermobility	No	No	Yes	No	No
Heart	Normal	Normal	Normal	ASDII, VSD	Normal
Muscle biopsy	Unspecific findings	Unspecific findings	Unspecific findings	Not performed	Not performed
Cranial MRI	No	No	No abnormalities	Semilobar holoprosencephaly	Atretic parietal encephalocele with associated minor anomalies of the cerebellar tentorium, and partial agenesis of corpus callosum
Epilepsy	No	No	No	Yes	No
EEG	No	No	No	Pathologic	Normal
Microcephalus	No	No	No	Yes	Borderline microcephaly (3rd centile)
Diabetes insipidus	No	No	No	Yes	No
Micropenis	N/A	N/A	No	Yes, cryptorchidism	No
Cleft lip/palate	No	No	No	Yes	No
BAEPs	N/A	N/A	Normal	No responses to an auditory stimulus (deafness)	N/A
Visual problems	No	No	No	Blindness	No
Facial dysmorphisms	Facial weakness, ptosis, high arched palate	Facial weakness, ptosis	Epicanthus, hypertelorism,	Bilateral cleft lip and palate, hypertelorism	Down slanted palpebral fissures, depressed nasal bridge
Others	Rough skin prone to hypertrophic scaring, frequent episodes of pneumonia, exercise induced myalgia, one hand Gower's manoeuvre	Exercise induced myalgia, one hand Gower's manoeuvre	Adducted thumbs	Bilateral contractures of hands and feet, small hypoplastic deep set nails, pituitary insufficiency	Occipital encephalocele, supernumerary nipple, single transverse palmer crease of the left hand
Birth weight, g (Perc./SD)	n.d.	n.d.	2790 (−1.17z)	3320 (50th)	n.d.
Birth length, cm (Perc./SD)	n.d.	n.d.	48	48 (10th–25th)	n.d.
Birth OFC, cm (Perc./SD)	n.d.	n.d.	34	34.5 (50th)	n.d.
Latest weight, kg (Perc./SD)	n.d.	n.d.	n.d.	6.165 (<3rd, −3.5z)	20.9 (59th)
Latest length, cm (Perc./SD)	n.d.	n.d.	n.d.	66 (<3rd, −3.5z)	117 (52nd)
Latest OFC, cm (Perc./SD)	n.d.	n.d.	n.d.	41 (<3rd, −2.3z)	49.5 (3rd)
Age at last clinical exam.	15 y	11 y	5 y and 6 mo	13 mo	5 y and 9 mo

ASDII = atrial septal defect type II; BAEPs = brainstem-evoked response audiometry; exam. = examination; mo = months; Perc. = percentile; SD = standard deviation; VSD = ventricular septal defect; y = years.

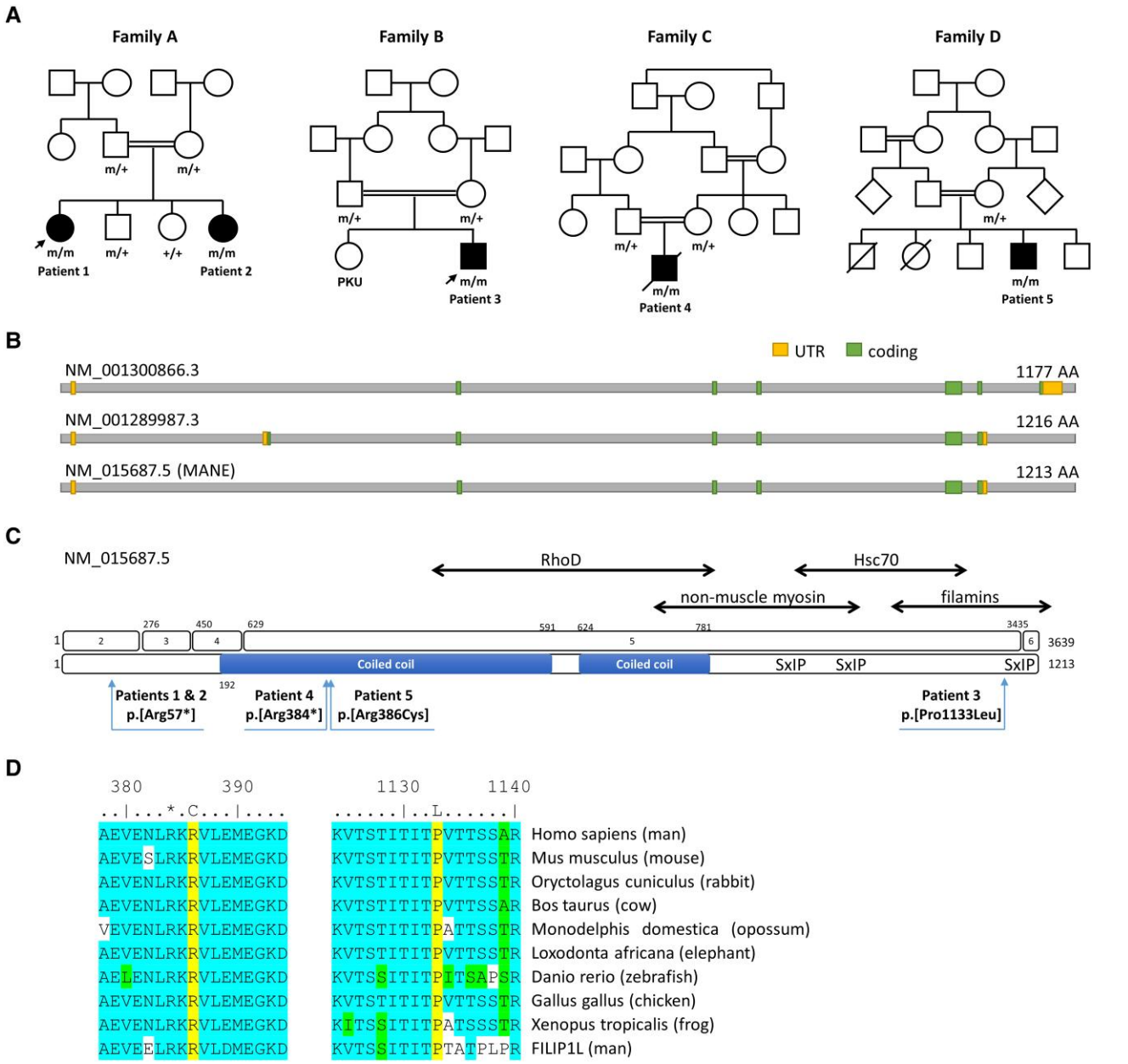

Figure 2 Pedigrees of patients of our FILIP1-cohort and schematic representation of FILIP1 gene and protein sequence along with distribution and conservation of identified variants. (**A**) Pedigrees of the consanguineous families of our four patients with identified *FILIP1*-variants. +/+ = wild-type, +/m = heterozygous, m/m = homozygous mutant. Arrows indicate patients for which muscle biopsies were studied. (**B**) Schematic representation of the FILIP1 protein encoded by different transcript isoforms including the MANE transcript NM_015687.5. (**C**) Schematic representation of the gene and protein sequence of *FILIP1*/FILIP1. Exons are numbered 1–6 (*top*). Pathogenic variants on protein level refer to the canonical/MANE transcript NM_015687.5 (*bottom*). The predicted coiled coil region is shown as a blue bar. Known binding partners are shown at the top. SxIP indicates the position of three putative EB1 and EB3 binding sites. Further amino acid regions of FILIP1 mediating interactions with RhoD, non-muscle myosin IIb, HSC70 and filamins are indicated by double-headed arrows. (**D**) Sequence alignments showing that Arg386 and Pro1133 (both yellow) are conserved between species and between FILIP1 and FILIP1L. *Arg384. Many of the amino acids flanking the variant are highly conserved (blue) or similar (green). UTR = untranslated region.

localized autophagic vacuoles containing pleomorphic membranous and granular material were identified [Fig. 3B(vi)].

Immunofluorescence studies carried out on cryosections of the quadriceps biopsy derived from Patient 3 revealed a co-localization of aggregated FLNc with FILIP1. Highly similar structures were also stained using an antibody specific for Xin actin-binding repeat-containing proteins and muscle damage markers Xin/XIRP2 (Fig. 3C) suggesting a co-localization of FILIP1 and Xin/XIRP2 in these structures. In contrast, desmin does not co-localize with FILIP1 in aggregates (Fig. 3C). These findings indicate that the missense variant causes the formation of pathological protein deposits of FILIP1 along with its interaction partner FLNc as well as with Xin/XIRP2, which indicate muscle damage and are well-established protein aggregation markers in myofibrillar myopathies.[25,26] However, desmin, a protein usually also affected by protein aggregate formation in myofibrillar myopathies, is not affected, indicating

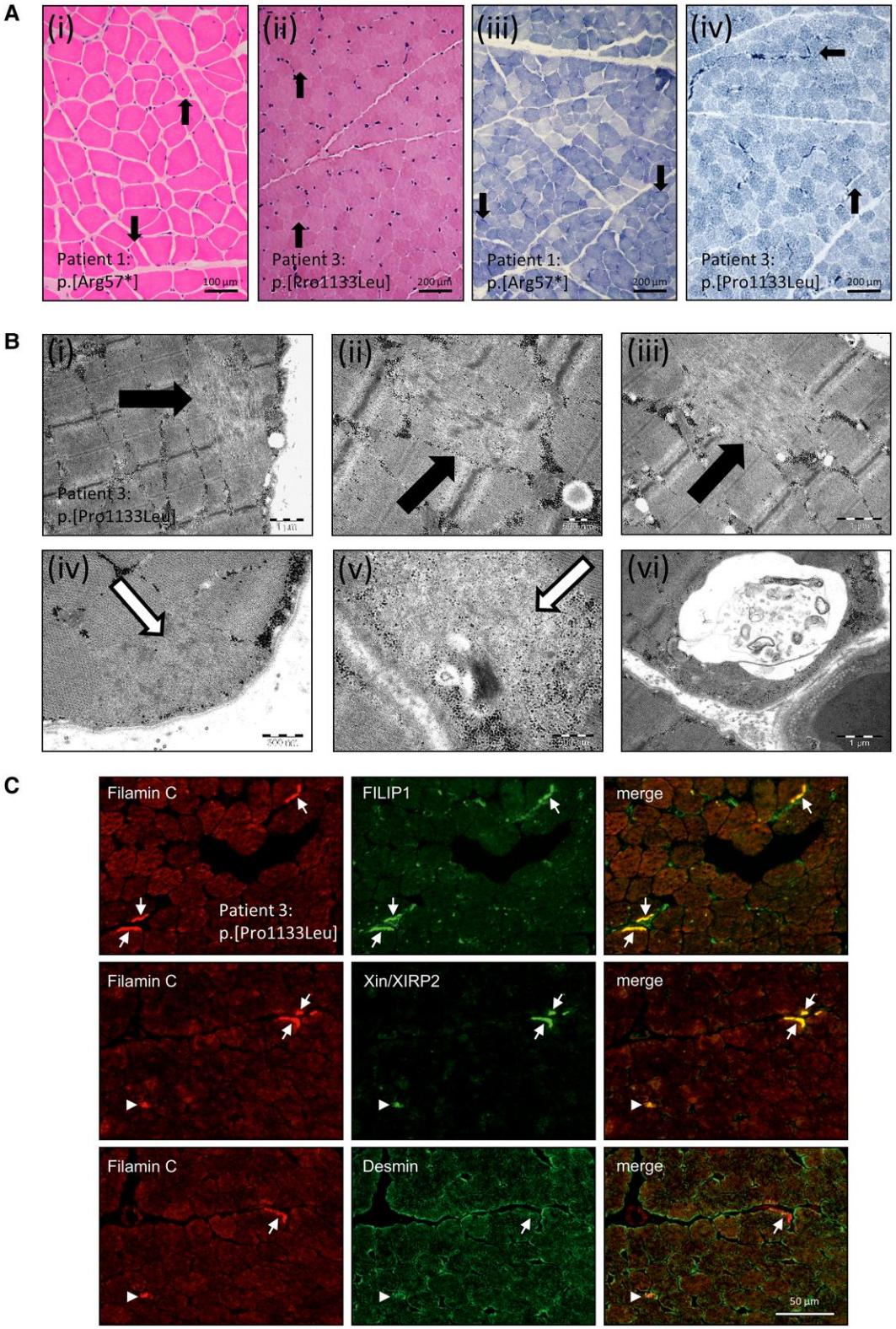

Figure 3 Microscopic studies including histology, electron microscopy and immunofluorescence on quadriceps muscle biopsy specimen of *FILIP1* patients revealing muscle cell vulnerability. (**A**) Histology of quadriceps muscle derived from Patients 1 and 3 reveals a very mild pathology with only few fibre-size variations [filled arrows in H&E stain (**i** and **ii**)] and no prominent pathological findings observed by NADH-TR stain (**iii** and **iv**); filled arrows indicate subsarcolemmal enrichment of mitochondria. (**B**) Electron-microscopic studies on the biopsy of Patient 3 revealed sarcomeric/myofibrillar disintegration as indicated by filled arrows (**i**–**iii**) and subsarcolemmal deposits of granular material as indicated by open arrows (**iv** and **v**) as well as presence of autophagic vacuoles (**vi**). (**C**) Immunolocalization of FLNc, Xin/XIRP2, FILIP1 and desmin in skeletal muscle fibres of Patient 3. Cryosections were double stained for antibodies against FLNc and FILIP1, Xin/XIRP2 or desmin, as indicated and reveal abnormal subsarcolemmal concentration of FLNc, FILIP1 and Xin/XIRP2, but not of desmin in several muscle fibres (arrows). Few small fibres were observed that are strongly positive for desmin, FLNc and Xin/XIRP2 (arrowheads).

biochemical differences to the typical aggregate composition in myofibrillar myopathies. To study the role of FILIP1 in the formation of aggregates in myofibrillar myopathies, triple-staining of FILIP1 with FLNc and Xin were carried out on muscle biopsy specimens derived from five patients with myofibrillar myopathies including desminopathy (c.1049G>C; p.[Arg350Pro]), dominant (c.2789_2800del; p.[Val930_Thr933del]) and recessive (c.1325C>G; p.[Pro442Arg]) filaminopathy, ZASPopathy (c.439G>A; p.[Ala147Thr]) and myotilinopathy (c.179C>T; p.[Ser60Phe]), respectively. These immunolocalization studies revealed a partial co-localization of FILIP1 with FLNc and especially with Xin and XIRP2 in all of these entities (Supplementary Fig. 1). Staining of cryosections derived from two valosin-containing protein (VCP) patients (c.464G>A; p.[Arg155His]) and two sporadic inclusion body myositis patients was also performed to address the distribution of FILIP1 in myopathies characterized by protein aggregation at a more general level. This approach also revealed partial colocalization of FILIP1 with FLNc in areas containing protein aggregates (Supplementary Fig. 2). FILIP1 was shown to be expressed in cultured differentiating myotubes and was found to bind non-muscle myosin and EB3, which are both important for skeletal muscle development.[27,28] Therefore, co-staining with anti-neonatal myosin was performed to analyse the abundance of FILIP1 in regenerating muscle fibres in the different neuromuscular disorders mentioned above and in Duchenne muscular dystrophy (DMD), a neuropaediatric disorder characterized by breakdown of cytoskeletal integrity. For DMD, quadriceps biopsies derived from two histologically and genetically confirmed patients were included. One patient underwent biopsy at the age of 5 years and presented with a hemizygous deletion of exons 45–50 in *DMD* while the other patient underwent biopsy at 2 years of age and presented with a hemizygous single nucleotide deletion c.8390+1delG in *DMD*. This approach revealed that FILIP1 is increased in regenerating fibres of myofibrillar myopathy, DMD and VCP patients (Supplementary Figs 2 and 3). Of note, some aggregate-containing fibres were also positive for neonatal myosin (MyHC), indicating ongoing regenerative processes within these fibres (Supplementary Figs 2 and 3).

In vitro and *in silico* studies of both FILIP1 missense variants

Pathogenic missense variants in proteins may change their solubility and/or make them more prone to degradation by proteolytic enzymes. We investigated both possibilities in biochemical assays using recombinant, bacterially expressed FILIP1 fragments. Although the expression level in bacteria of recombinant p.[Pro1133Leu], the homozygous variant in Patient 3, was the same as the wild-type protein (Fig. 4A), it was more difficult to purify the mutant protein. A comparison of the solubility of wild-type and mutant proteins under non-denaturing conditions revealed that 90.9 ± 0.9% of the wild-type protein was soluble in lysis buffer, while under the same conditions, only 22 ± 4.3% of the mutant protein was soluble [$P < 0.0001$; Fig. 4B(i and ii)]. This finding demonstrates the significantly reduced solubility and consequently increased aggregation propensity of the mutant protein. The potential of gross alterations in protein structure was further investigated by treatment of both proteins with the protease thermolysin, which preferentially cleaves proteins before leucine and phenylalanine residues. Gel-electrophoretic analysis of the digests revealed that under the same conditions a significantly larger part of the mutant protein was digested for most incubation conditions when compared to the wild-type protein [Fig. 4C(i and ii)]. After 40 min digestion, for example, only 47.1 ± 6.0% of the mutant protein remained undigested, while 64.7 ± 5.0% of the wild-type protein was still intact (mean ± standard deviation, $P < 0.001$). Together, these results demonstrate that the p.[Pro1133Leu] variant in FILIP1 causes decreased solubility of the protein and increased susceptibility to proteolysis in solution, indicating that this variant does affect protein structure and stability. In contrast, purification of the p.[Arg386Cys] variant did not lead to any solubility differences (data not shown), and significant differences in susceptibility to thermolysin [Fig. 4D(i and ii)] and trypsin [Fig. 4E(i and ii)] were not detected.

As FILIP1 contains a large region that is predicted to form coiled coils, we performed an *in silico* analysis of the effect of the p.[Arg386Cys] variant using the COILS Server at embnet.vital-it.ch. Applying a window width of 14, extended coil regions were predicted in wildtype FILIP1 amino acids 189–786, interrupted by short regions not predicted to contain coils (Fig. 4F). In contrast, the p.[Arg386Cys] variant was predicted to completely destroy one of the coil-containing regions (Fig. 4F), thus further supporting a structural effect of the amino acid substitution on the FILIP1 protein.

Given that FILIP1 was predicted to form dimers when expressed in cultured COS-7 cells,[29] we next analysed the ability of both 70 kDa FILIP1-coil variants to dimerize *in vitro* using cross-linking assays. After only a short incubation with EGS, not only dimers (~140 kDa), but also 280 kDa tetramers of both recombinant proteins were formed, the amount of which increased with longer incubation times. Although the p.[Arg386Cys] variant was predicted to lack a part of the coiled coil region, no significant differences between this variant and wildtype FILIP1 in the ability to dimerize and tetramerize were detected [Fig. 4G(i and ii)]. Uncropped versions of the findings mentioned above are shown in Supplementary Fig. 4.

In silico studies using PremPS predict that both missense variants alter the non-covalent interactions within FILIP1. The variant p.[Arg386Cys] is predicted to maintain all existing intramolecular interactions in the wild-type protein, but causes a novel Van der Waals interaction between Cys386 and Met390 (Supplementary Fig. 5). In the wild-type form of the FILIP1 protein there is no non-covalent interaction at Pro1133; however, the p.[Pro1133Leu] variant is predicted to induce a hydrophobic interaction between Leu1133 and Thr1135 (Supplementary Fig. 5). Taken together, these results are indicative of a change in structure due to the amino acid substitutions identified in Patients 3 and 5 and thus support the findings from our biochemical experiments and lend credence to the hypothesis that they are pathogenic.

In addition, protein stability was quantified through the unfolding Gibbs free energy changes (DDG, kcal/mol), where a positive score is indicative of decreased stability and a negative score indicates increased stability. Interestingly, the two missense variants are predicted to have opposite effects on the stability of FILIP1: p.[Arg386Cys] is predicted to be a destabilizing variant (DDG: 0.46) whereas p.[Pro1133Leu] is predicted to be a stabilizing variant (DDG: −0.18). The latter finding accords with our findings obtained by recombinant protein expression in bacteria. Although these amino acid substitutions do not reach the threshold for 'highly destabilizing/stabilizing mutations' ($\Delta\Delta G$ of greater than 1 (destabilizing) or less than −1 (stabilizing)[24]), these changes nevertheless predict that both missense mutant proteins have altered stability.

Clinical comparison of *FLNA*, *FLNC* and *FILIP1* cases

Prompted by the fact that FILIP1 interacts with FLNa and FLNc, two proteins for which pathogenic variants in the corresponding genes

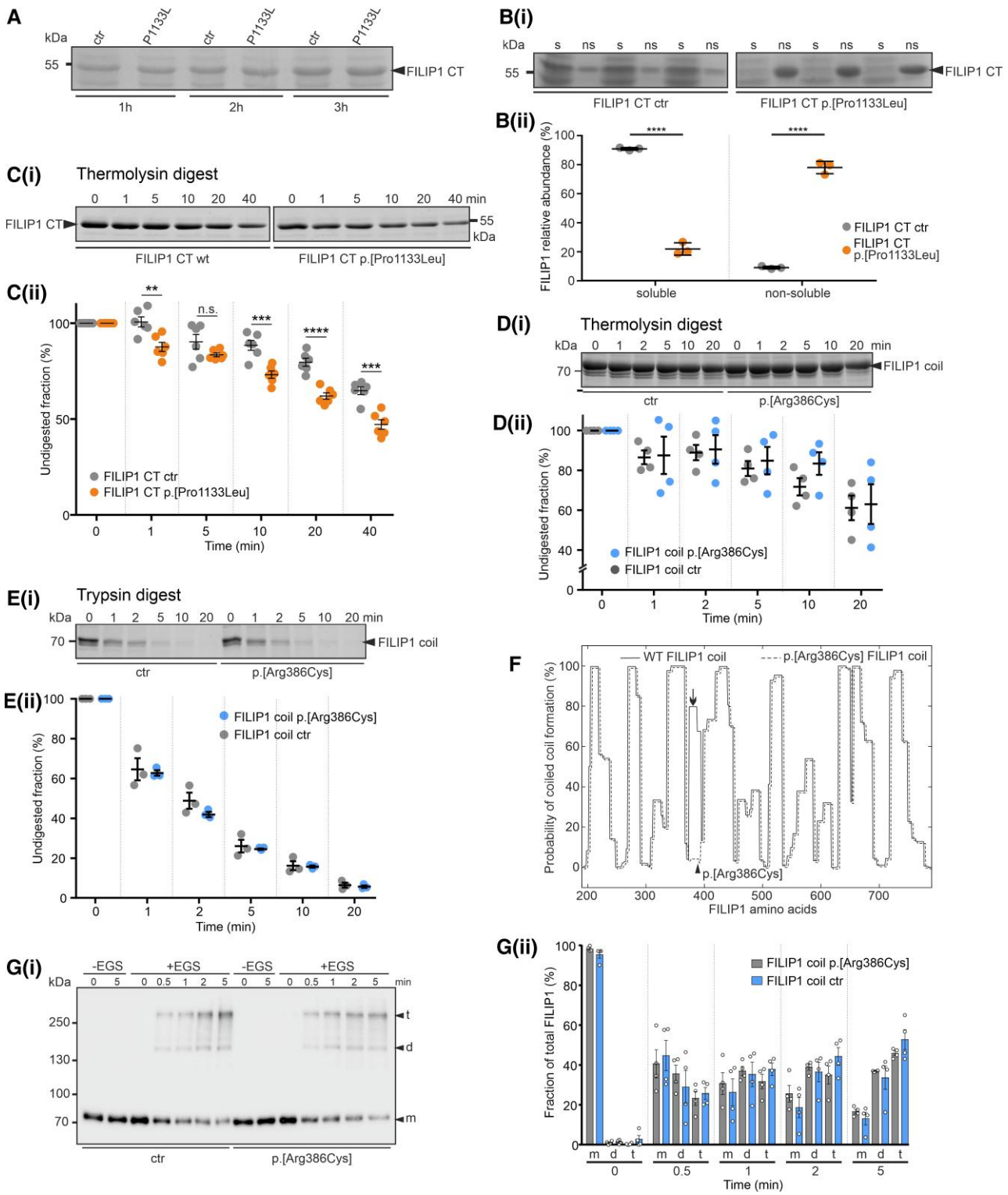

Figure 4 ***In vitro*** **studies addressing stability and solubility of recombinant FILIP1 CT and FILIP1 coil constructs.** (**A**) SDS-PAGE analysis of total extracts of bacteria 1, 2 or 3 h after induction of wild-type (wt) or mutant (p.[Pro1133Leu]; mut) protein expression [carboxyterminus (CT), amino acids 776–1177]. Note that equal levels of protein (arrowhead) are expressed. [**B(i** and **ii)**] Investigation of the solubility of wt and mutant FILIP1 CT proteins (arrowhead). Note that the mutant protein is found almost exclusively in the non-soluble fraction (ns), whereas approximately 80% of the wt protein is soluble (s). [**C(i** and **ii)**] Investigation of protease susceptibility by native, limited thermolysin digestion: wt and mut FILIP1 CT fragments were treated with the protease thermolysin for 0–40 min, as indicated above each lane. Samples were analysed by SDS-PAGE. Note that significantly higher levels of the p.[Pro1133Leu] variant are digested after almost all incubation times, indicating decreased stability of the mutant protein. (**D** and **E**) Investigation of protease susceptibility of both FILIP1 coil variants by native, limited thermolysin [**D(i** and **ii)**] or trypsin [**E(i** and **ii)**] digestion. Recombinantly expressed FILIP1 coil fragments were treated with either thermolysin or trypsin for 0–20 min, as indicated above each lane. Samples were analysed by SDS-PAGE. Both variants do not show any significant differences in protease susceptibility. (**F**) Prediction of coiled coil formation in the central part of FILIP1. Amino acids

(continued)

were linked to the manifestation of symptoms also identified in our cohort of patients presenting with recessive *FILIP1* variants, a clinical comparison between these phenotypes was carried out. This comparison of the clinical presentations associated with variants in *FLNA*, *FLNC* and *FILIP1* is presented in Supplementary Table 4 and shows partially overlapping clinical phenotypes.

FILIP1 is expressed in skin fibroblasts

The expression of *FILIP1* in cultured fibroblasts was investigated by reverse-transcription PCR (RT-PCR). In both control fibroblasts and fibroblasts derived from Patient 3, expression of *FILIP1* mRNA was identified (Fig. 5A). Furthermore, the expression solely of the c.3398C>T variant in the patient cells was confirmed by restriction digestion of the amplicons using the *BshTI* enzyme, which only cuts the cDNA derived from the control fibroblasts (Fig. 5A). Uncropped versions of the agarose gels are shown in Supplementary Fig. 4. These results accord with the *in silico* predictions established by GTEx-interrogation (Fig. 5B) and more specifically with the results of analysis of RNA expression in isolated skin fibroblasts from the Human Protein Atlas (https://www.proteinatlas.org/ENSG00000118407-FILIP1/single + cell + type/skin).

Expression of mutant *FILIP1* alters the proteomic signature of skin fibroblasts

We investigated the proteomic signature of skin fibroblasts derived from Patient 3 (p.[Pro1133Leu]) using a label-free LC-MS/MS approach (Fig. 5C) and quantified 1196 proteins, of which 106 were statistically significantly dysregulated: 45 proteins were increased and 61 decreased (Fig. 5D and Supplementary Table 1). Of note, FLNc was identified among the decreased proteins (Fig. 5E). A gene ontology (GO)-term-based *in silico* analysis of dysregulated proteins was performed to elucidate the biological processes and subcellular compartments affected by the p.[Pro1133Leu] amino acid substitution in FILIP1. The results of this investigation revealed that upregulated proteins are involved in the organization of the extracellular matrix, cell adhesion, rRNA processing and protein translation, and protein heterotrimerization, as well as TGFβ secretion (Fig. 5F). In contrast, downregulated proteins are involved in metabolic processes, modulation of apoptosis, regulation of cell growth and proliferation, receptor-mediated endocytosis and the integrin-mediated signalling pathway (Fig. 5F). Focusing on subcellular compartments, increased proteins are mainly resident within the extracellular matrix and the endoplasmic reticulum (ER) along with the ER-Golgi intermediate compartment, focal adhesion sites, ribosomes and the sarcolemma (Fig. 5F). However, decreased proteins mainly localize to extracellular exosomes, the actin cytoskeleton, focal adhesion sites, lysosomes, endocytotic vesicles and the sarcolemma (Fig. 5F). Thus, the results of this *in silico* analysis suggest that the variant has an effect on diverse biological processes as well as on subcellular structures beyond the cytoskeleton. Nevertheless, protein dysregulation in fibroblasts from Patient 3 clearly indicate that the cellular cytoskeleton is affected not only by the above-mentioned decrease of FLNc but also by downregulated quantities of myosin phosphatase Rho-interacting protein (MPRIP; accession: Q6WCQ1), ezrin (EZRI; accession: P15311), synaptopodin-2 (SYNP2; accession: Q9UMS6) and desmoplakin (DESP; accession: P15924) as well as by increase of desmin (DES; accession: P17661), an intermediate filament protein (Supplementary Table 3).

Focusing on dysregulated proteins known to be causative of neurological and neuromuscular diseases, some of the upregulated proteins have previously been shown to be causative of muscle diseases [desmin (DES; accession: P17661], collagen VI (COL6; accession: P12111, P12110, P12109), alpha-B-crystallin (CRYAB; accession: P02511) and basement membrane-specific heparan sulfate proteoglycan core protein/perlecan (PGBM; accession: P98160), neuropathic disease [neprilysin (MME); accession: P08473] and a neurodevelopmental disorder [cytoplasmic serine-tRNA ligase (SARS1); accession: P49591]. Some of the decreased proteins are also linked to muscle diseases including filamin-C (FLNc; accession: Q14315), delta-sarcoglycan (SGCD; accession: Q92629) and lysosomal alpha-glucosidase (GAA; accession: P10253). CD59 glycoprotein (CD59; accession: P13987) decreased in patient derived fibroblasts is associated with a neuropathic disease. Moreover, decreased proteins such as *N*-sulphoglucosamine sulphohydrolase (SPHM; accession: P51688) and a serine protease (HTRA1; accession: Q92743) are linked with neurodegenerative diseases as well as developmental delay/intellectual disability including aldehyde dehydrogenase family 3 member A2 (ALDH3A2; accession: P51648).

The information above was obtained from UniProt (www.uniprot.org). In summary, the proteomic signature obtained from skin fibroblasts reflects proteomic changes that are likely to occur in muscle and nervous tissue, which seem to be most severely affected by FILIP1 variants.

Cytoskeletal vulnerability in *FILIP1*- and *FLNC*-mutant fibroblasts

We hypothesized that p.[Pro1133Leu]-FILIP1 mutant fibroblasts display a more pronounced cytoskeletal vulnerability *per se*. To address this assumption, to validate our proteomic findings and to further investigate the role of FLNa in FILIP1opathy, fibroblasts derived from controls, from Patient 3 and from a patient affected myofibrillar myopathy caused by the dominant *FLNC* c.4984C>T; p.[Gln1662Ter] variant serving as a disease control, were analysed by immunofluorescence microscopy. To calculate the percentage of fibroblasts presenting with altered immunostaining in terms of reduced protein abundance and/or irregular distribution, 20 cells were analysed per condition. These studies revealed a reduced abundance of FLNc accompanied by the presence of focal cytoplasmic dots immunoreactive for FLNc in FILIP1-patient-derived

Figure 4 (Continued)
189-786 of both, FILIP1 and the p.[Arg386Cys] variant, are predicted to form extended coiled coil secondary structures when submitted to the COILS Server at embnet.vital-it.ch. Note however, the predicted total loss of coiled coil formation propensity of the region affected by the variation (arrow). The position of Arg386 is indicated by an arrowhead. The graph of the mutant protein was deliberately shifted a few pixels, to be able to distinguish both graphs. [**G(i** and **ii)**] Chemical cross-linking experiments using wt FILIP1 coil and the p.[Arg386Cys] variant. Assays were performed in the absence (–EGS) or presence (+EGS) of EGS. Reaction mixtures were analysed by western blotting using specific antibodies against the EEF-immunotag of the constructs. Without the cross-linker EGS, only monomers (m) of the constructs were detected. In the presence of EGS, within 0.5 min both variants were also found as dimers (d) or tetramers (t). With extension of the incubation time, the relative amount of protein found as tetramers increased to up to 45–65% of the total amount of protein. No significant differences were observed between both variants. Panels **A–E** and **G** contain cropped gels or blots. For full-size versions, see Supplementary Fig. 4. All data are the result of three to six independent experiments. All statistics were performed using GraphPad Prism and paired *t*-test. Data are shown as mean ± SEM. $^{**}P < 0.01$; $^{***}P < 0.001$; $^{****}P < 0.0001$.

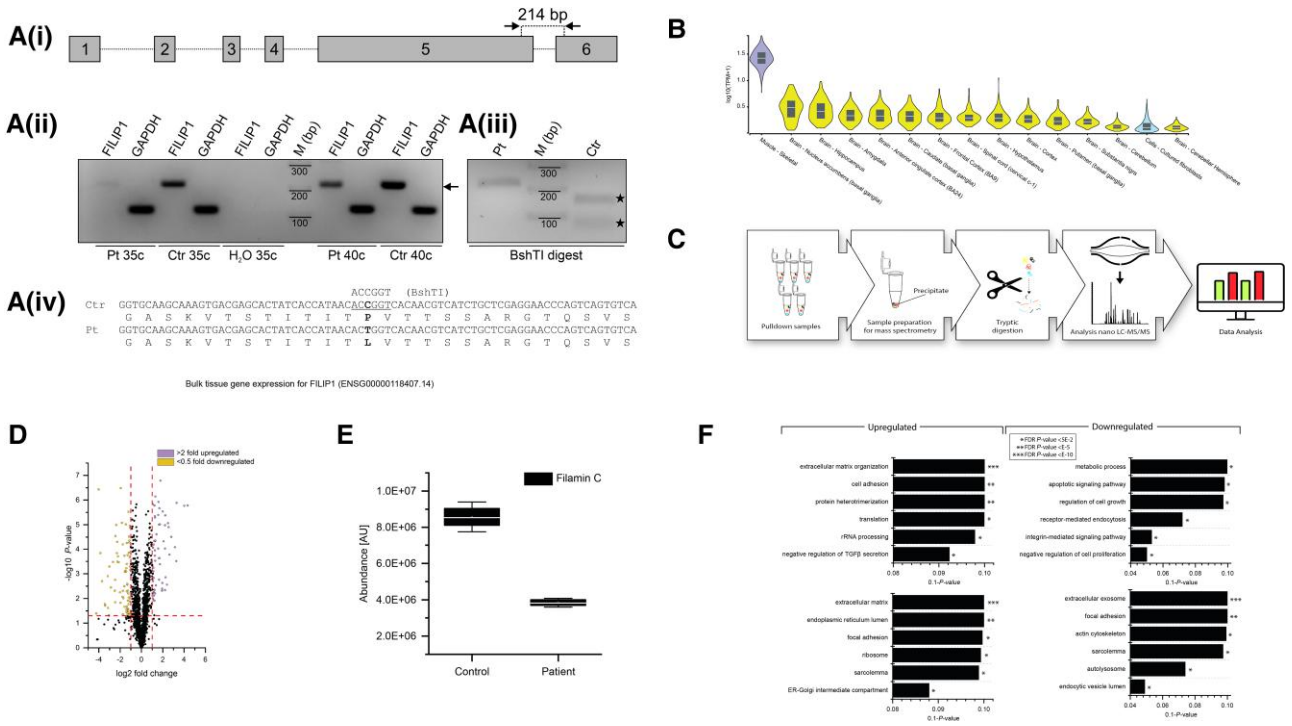

Figure 5 Investigation of FILIP1 expression and subsequent proteomic profiling of fibroblasts derived from FILIP1 Patient 3 p.[Pro1133Leu]. [**A(i)**] cDNA prepared from RNA isolated from skin fibroblasts from our c.3398C>T; p.[P1133L] patient (Pt) or control (Ctr) fibroblasts, was amplified using oligonucleotides that amplify the indicated 214 bp fragment of *FILIP1* mRNA or *GAPDH* mRNA. [**A(ii)**] Both primer pairs amplify the expected *FILIP1* (arrow) and *GAPDH* fragment from Pt and Ctr fibroblasts using 35 or 40 cycles (c). [**A(iii)**] Analysis of the sequence of Ctr and Pt FILIP1 cDNA reveals the loss of a BshTI restriction site in Pt cDNA. [**A(iv)**] Schematic presentation of BshTI digestion of Pt and Ctr cDNA. Ctr cDNA is completely digested (filled stars), while Pt cDNA is still intact, confirming homozygous expression of the c.3398C>T variant in skin fibroblasts of our patient. Uncropped versions of the gels are shown in Supplementary Fig. 4. (**B**) Confirmed FILIP1 expression by *in silico* based GTex-analysis in fibroblasts (blue). (**C**) Schematic representation of the applied workflow. (**D**) Volcano plot of proteomic findings; yellow dots represent proteins showing a significant decrease whereas purple dots represent proteins with a significant increase in abundance. The *x*-axis reflects the magnitude of fold-changes (base 2) and the *y*-axis represents the negative log of the *P*-value (base 10). (**E**) Box plot-based representation of decreased FLNc abundance in FILIP1-patient derived fibroblasts compared to controls. (**F**) GO-term-based representation of the six most (statistically significant) affected biological processes and subcellular compartments/structures depicted for the increased and decreased proteins, respectively.

fibroblasts, confirming our proteomic findings (Fig. 6A). Interestingly, *FLNC*-mutant fibroblasts presented with a more pronounced perinuclear FLNc-immunoreactivity compared to control cells and none of these cells presented with reduced FLNc-abundance as observed in fibroblasts derived from the FILIP1 patient. Cytoplasmic FLNc-immunoreactive dots were even less present in *FLNC*-mutant fibroblasts than in controls (Fig. 6A). Whereas both, FLNC- and FILIP1-mutant fibroblasts, show a general reduction of cytoplasmic FLNa-staining compared to control cells, cytoplasmic dots immunoreactive for FLNa were only found in FILIP1-mutant cells (Fig. 6A). Altered immunostaining in terms of reduced cytoplasmic abundance of FILIP1 was identified in fibroblasts derived from both patients (Fig. 6A). Given that affected chaperone alpha-B-crystallin has been linked to the pathophysiology in filaminopathies[30] and we here showed that this chaperone is dysregulated in fibroblasts from Patient 3, we studied its distribution in fibroblasts of both patients. Altered immunostaining in terms of the presence of focal cytoplasmic enrichment was observed in fibroblasts derived from both patients (Fig. 6A). In the FILIP1opathy fibroblasts, these enrichments localized to the ends of cellular processes from which filopodia originate (Fig. 6A). Staining of the actin cytoskeleton by phalloidin revealed a statistically significant reduced COI in fibroblasts derived from the filaminopathy patient but not the FILIP1opathy patient compared to controls (Fig. 6B and C). Given that FILIP1 has been linked to cell migration,[31] a process depending on actin-rich structures called filopodia that protruding from the lamellipodial actin network,[32] we next examined these structures in phalloidin-stained fibroblasts. No differences in number and branching of filopodia were detected between control and patient fibroblasts (Supplementary Fig. 6).

In addition, we exposed the above-mentioned *in vitro* models to 0.05 µg/ml µM cytochalasin-D for 90 min. The effect of treatment was monitored by light and immunofluorescence microscopy (FITC-phalloidin to visualize actin), and prior cellular activity was investigated by measuring cellular metabolic activity as an indicator of cell viability, proliferation and cytotoxicity using an MTT-assay. Light microscopy studies frequently revealed a rounded cell shape and immunofluorescence studies of the actin cytoskeleton revealed disintegration of actin bundling upon cytochalasin-D exposure in control and patient fibroblasts (Supplementary Fig. 7A) confirming the deleterious effect of drug exposure on actin cytoskeletal integrity. Although the results of our MTT-assay revealed decreased viability in *FLNC*- (statistically not significant) and *FILIP1*-mutant fibroblasts (statistically significant) compared to controls under basal conditions (non-treated), the applied dose of cytochalasin-D for 90 min did not alter the metabolic activity (reflecting the number of viable cells) in fibroblasts derived either from controls or from the patients (Supplementary Fig. 7B). In contrast, an increased cytotoxic effect was observed in fibroblasts derived from the FILIP1-patient

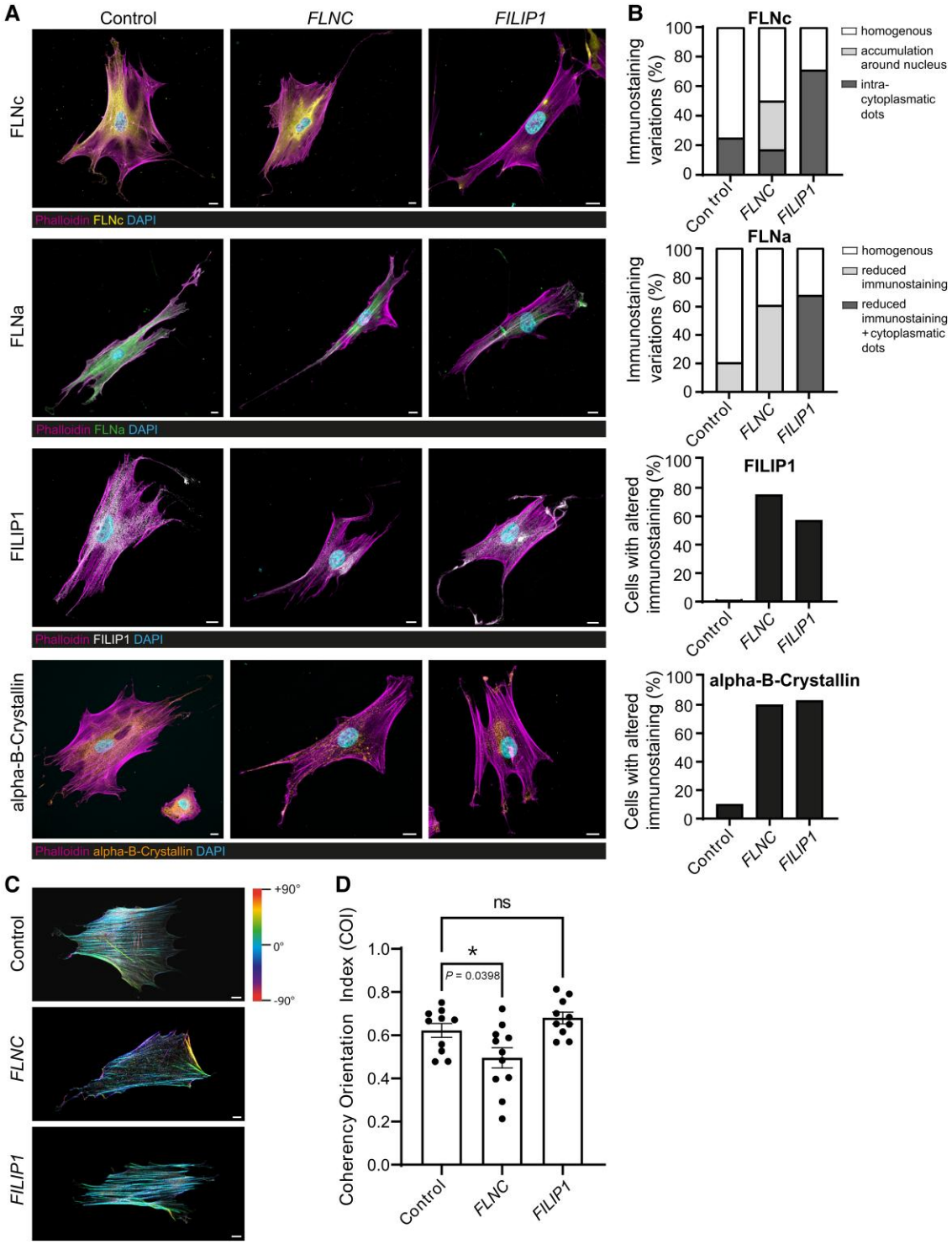

Figure 6 Immunofluorescence studies to investigate the spatial distribution of FLNc, FLNa, FILIP1 and alpha-B-crystallin, along with actin fibre orientation in *FLNC*- and *FILIP1*-mutants, as well as control fibroblasts. (**A**) While control fibroblasts show a homogeneous cytoplasmic distribution of FLNc (yellow), FLNa (green), FILIP1 (white) and alpha-B-crystallin (orange), a marked reduction of FLNc and FLNa is observed in fibroblasts derived from FILIP1opathy Patient 3.These proteins and also alpha-B-crystallin showed a condensed, dot-like localization in fibroblasts of this patient, that were more frequently localized close to cellular processes than in control cells. In fibroblasts derived from a filaminopathy patient, FILIP1-immunoreactivity is also reduced. In these fibroblasts, alpha-B-crystallin (orange) also presents a condensed immunoreactivity compared to controls but without frequent localization to cellular processes. FLNa immunoreactivity is similar to that observed in control fibroblasts. FLNc immunoreactivity is more prominent in the perinuclear region compared to FILIP1opathy and control fibroblasts. (**B**) Percentage of fibroblasts identified with altered protein abundances and/or distribution based on immunofluorescence staining. (**C**) Circular colour map coding of actin filament orientation visualized by FITC-phalloidin-staining, shows a higher variance in filaminopathy fibroblasts compared to FILIP1opathy and control fibroblasts. (**D**) Higher actin filament variances result in a significantly decreased cytoskeletal coherency in filaminopathy fibroblasts compared to control and FILIP1opathy fibroblasts. $n = 10–11$ fibroblasts for each genotype. Mean ± SEM, $^*P = 0.0398$, D'Agostino and Pearson test for normal distribution followed by one-way ANOVA and Dunnett's multiple comparison test. Scale bars = 10 µm.

compared to both control and *FLNC*-mutant fibroblasts both displaying reduced cytotoxicity (Supplementary Fig. 7C).

Discussion

FILIP1 codes for a structural protein interacting with the actin-cross-linking proteins FLNa and FLNc, two proteins for which pathogenic variants in the corresponding genes are already linked to the manifestation of neurological symptoms. FILIP1 is highly expressed in skeletal and cardiac muscle as well as in the nervous system. The protein is also located in the cytoskeleton of the cell.[4,33] The expression pattern of FILIP1 in skeletal muscle and the nervous system is in line with the clinical manifestation of pathogenic variants in the corresponding gene identified in this study: in five patients from four unrelated consanguineous families, bi-allelic variants including two nonsense and two missense variants were associated with variable congenital neurological symptoms including brain malformations and a neuromuscular disorder. Hypotonia, delayed achievement of motor milestones, delayed speech development and intellectual disability are consistent features observed in patients with recessive *FILIP1* variants. The clinical spectrum is accompanied by shared facial dysmorphic features including ptosis, epicanthus, downslanted palpebral fissures, hypertelorism, broad root of the nose/depressed nasal bridge and high arched palate, forming a recognizable 'Gestalt'. Of the five patients described, the one presenting with the most severe phenotype (Patient 4; p.[Arg384*]) died at the age of 13 months. In view of the consanguinity of the parents, the very severe clinical presentation of this patient might be caused by additional genetic variants that remained undetected. No pathogenic variant in other genes associated with neurological phenotypes were identified in this patient by exome sequencing. The description of additional patients with pathogenic variants in *FILIP1* will help to better define the clinical presentation and to elucidate genotype-phenotype correlations in the future.

FILIP1 was shown to bind non-muscle myosin and EB3,[27,28] both of which are associated with the cytoskeleton and involved in neuritogenesis and skeletal muscle development. Mice lacking *Filip1* show abnormal dendritic spine morphology associated with disturbed localization of non-muscle myosin 2b. Interestingly, EB3 is involved in neuritogenesis and normal development of dendritic spines.[33] To our knowledge, skeletal muscle function was not studied in these mice.

As an actin-cross-linking protein, FLNc is involved in reorganizing the actin cytoskeleton in response to signalling events and dominant *FLNC* variants are associated with an adult-onset myofibrillar myopathy characterized by disintegration of the sarcomeric Z-disc and myofibrils, and replacement of the normal myofibrillar markings by small dense granules, larger hyaline masses or amorphous material (MIM:609524). FLNc accumulation was recently also described in a neuropaediatric patient; the first case affected by a recessive homozygous *FLNC* variant and presenting with a congenital onset of muscular symptoms,[7] while most *FLNC*-related myofibrillar myopathy patients have a disease onset much later in life. Interestingly, a decrease in FLNc abundance was identified in fibroblasts derived from *FILIP1*-patient 3 with a variant in the filamin-binding region, while FLNc-containing aggregates were observed in muscle fibres of the same patient. This might indicate a direct impact on functional FILIP1. This assumption is supported by the results of ultrastructural studies revealing Z-disc alterations and myofibrillar disintegration and the presence of autophagic deposits in the subsarcolemmal region. These combined immunofluorescence and ultrastructural findings hint at the pathological hallmarks observed in myofibrillar myopathies. However, the light and electron microscopic findings observed in *FILIP1*-mutant muscle are only mildly pathological, and no match to what is typically found in myofibrillar myopathies, which are characterized by more widespread myofibrillar breakdown and severe accumulations of granulofilamentous material. Myopathological studies on further FILIP1-patients are needed to obtain a broader understanding of the spectrum of these findings. However, investigations of FILIP1 abundance and localization in biopsies derived from patients affected by genetically confirmed myofibrillar myopathies revealed a partial co-localization of FILIP1 within aggregates, suggesting a role of the protein in their composition. This partial co-localization might indicate a metastable subproteome, where aggregates mature and saturate in a dynamic way.[34]

To answer the question of whether FILIP1 plays a more general role in aggregate formation within muscle cells, we analysed biopsies of patients with genetic and acquired protein aggregate myopathy (PAM: VCP-related and sporadic inclusion body myositis). The results of these immunofluorescence studies also revealed a partial co-localization of FILIP1 within protein aggregates immunoreactive for FLNc and thus suggest a more general role of FILIP1 in protein aggregate formation under myopathological conditions rather than a specific impact in the etiopathology of myofibrillar myopathies. Comprehensive studies focusing on further PAMs are required to confirm this assumption and investigation of animal models in this context would allow the role of FILIP1 in the maturation of these aggregates to be addressed more specifically. Of note, the results of our immunofluorescence studies also showed an increased abundance of FILIP1 in regenerating fibres from patients with different neuromuscular disorders, a finding which is in line with the expression of FILIP1 during *in vitro* muscle cell differentiation[6] and its interaction with EB3 and non-muscle myosin, two proteins known to be involved in early muscle cell differentiation.[27,28] Hence, our data support the assumption that FILIP1 plays an important role in muscle cells in health and disease.

Reported chromosome 6q microdeletion syndromes include deletion of the *FILIP1* gene and associated phenotypic features comprise intellectual disability, facial dysmorphism, skeletal deformities and hypotonia.[35] In addition, a *de novo*, possibly damaging variant in *FILIP1* was found in a schizophrenia proband.[36] As presented in Supplementary Table 4, *FILIP1*-associated disease shares phenotypic features with both *FLNA* and *FLNC*-associated conditions: patients with *FLNA* and *FILIP1* variants share the neurodevelopmental delay (intellectual disability, language and motor delay), brain malformations, hearing loss, skeletal abnormalities and facial dysmorphisms as well as congenital onset and non-progressive course. These features are not seen in *FLNC*-associated conditions. In a more detailed comparison of dysmorphisms, patients with *FLNA* and *FILIP1* variants both exhibit down-slanted palpebral fissures, hypertelorism and wide or flat nasal bridge. High arched palate, ptosis and cleft palate were described in a few patients each. Comparing the skeletal abnormalities, both *FLNA* and *FILIP1* patients may present with scoliosis and elbow, knee and finger contractures and may also have increased joint laxity. In contrast, *FLNC* and *FILIP1* patients share the myopathic phenotype, which is absent in patients with *FLNA*-associated conditions. *FLNC*- and *FILIP1*-associated myopathies are associated with normal to mildly elevated CK. Congenital onset as seen in *FILIP1* has only been described in a single *FLNC* patient with myofibrillar myopathy subtype to date. Usually, patients with myofibrillar subtype 5 of *FLNC*-associated disease present with slowly progressive proximal weakness

affecting the lower limbs more than the upper limbs. Distal muscles may also be affected. In a subtype of *FLNC*-associated distal myopathy (OMIM:614065), patients have affected distal upper and lower limbs with progression to proximal weakness. This pattern is similar in one of our *FILIP1* patients who has mild weakness of proximal upper limbs in addition to proximal and distal lower limb involvement. However, a reliable assessment of muscle strength is often not feasible in children with FILIP1opathy because of their young age and mental retardation.

The proteomic signature of fibroblasts derived from *FILIP1* patient 3 revealed dysregulation not only of FLNc but also of a range of other proteins associated with neurological disorders with symptoms also observed in our patients: for instance, ALDH3A2, which is decreased in *FILIP1*-patient derived fibroblasts. Bi-allelic variants within the corresponding gene *ALDH3A2* are associated with a combination of severe intellectual disability, spastic di- or tetraplegia, congenital ichthyosis, seizures and speech defects (OMIM:270200). Further studies *in vitro* or in animal models are required to confirm such a correlation and to link these symptoms to a direct molecular interplay between FILIP1 and ALDH3A2.

Proteomic findings obtained on fibroblasts derived from Patient 3 already suggested cytoskeletal vulnerability by dysregulation of FLNc and desmin, two proteins responsible for subtypes of myofibrillar myopathies, as well as an increase in alpha-B-crystallin, a sarcoplasmic chaperone which has already been linked to the pathophysiology of filaminopathies.[37] Our confirmational immunofluorescence studies showed altered FLNc as well as a comparable pathogenic immunoreactivity of FILIP1 and alpha-B-crystallin in *FLNC*-mutant fibroblasts and cells derived from Patient 3 compared to controls, thus indicating similar cytoskeletal vulnerability, a molecular finding which might suggest similar muscle cell vulnerability in cases where pathogenic variants are present in the corresponding genes. Given that FILIP1 interacts with FLNa and our FILIP1 patients share clinical features observed in patients affected by pathogenic *FLNA* variants, we next investigated FLNa immunoreactivity, also including *FLNC*-mutant fibroblasts as a disease control to address the question of whether perturbed FLNa abundance and/or distribution only occurs in *FILIP1*-mutant fibroblasts and thus might explain the presence of extra-muscular symptoms. Indeed, while fibroblasts derived from both patients present with a generalized reduction in immunoreactivity, only FILIP1-mutant fibroblasts show the presence of cytoplasmic dots immunoreactive for FLNa. Thus, in accordance with a direct interaction of FILIP1 with FLNa, one might postulate that pathogenic distribution in terms of aggregate-formation of FLNa in *FILIP1*-mutant cells contributes to the underlying pathophysiology and clinical manifestation of FILIP1opathy. This microscopic finding might also accord with the absence of *FLNA*-associated symptoms in *FLNC*-patients. However, other possible explanations include (i) restricted or tissue-specific expression of both proteins; (ii) additional functions of FILIP1 in other cell populations such as neurons which might cause the extra-muscular symptoms based on tissue-specific pathophysiology; and (iii) an increased tolerance of *FLNC*-mutant cells to cytoskeletal perturbations. The latter assumption is supported by the results of our combined immunofluorescence, viability and cytotoxicity studies in which FILIP1-mutant fibroblasts showed a reduction in cell fitness accompanied by increased cytotoxicity upon cytochalasin-D exposure compared to *FLNC*-mutant cells which presented with a reduced coherency orientation index of actin filaments. In this context, it is important to note that treatment of both control and *FLNC*-mutant fibroblasts with 0.05 µg/ml µM cytochalasin-D for 90 min resulted in a decrease of cytotoxicity. This effect is most likely caused by the activation of cellular compensatory mechanisms, a stress response which has already been described in cytochalasin-D exposed fibroblasts.[38] However, further studies including different cell populations are needed to confirm this assumption and to identify potential rescue mechanisms in *FLNC*-mutant cells which might explain the differences.

Our fibroblast-based cell model from Patient 3 confirmed the molecular interplay of FILIP1 and FLNc and the impact of the recessive *FILIP1* variants was seen in muscle fibres derived from the same patient. Unfortunately, patient-derived material is rarely available to directly investigate the pathogenicity of ambiguous variants such as the amino acid substitutions identified in FILIP1. Here, our *in vitro* studies focusing on the solubility and stability of bacterially expressed FILIP1 variants, combined with *in silico* analysis of secondary structure (in this case coiled coil formation) proved to be a fruitful combination of methods allowing us to evaluate the pathogenicity of amino acid substitutions in FILIP1.

However, the manifestation of a broad spectrum of neurological (and dysmorphic) features associated with recessive *FILIP1* variants remains surprising. Apart from altered protein solubility and effects on protein structure, we cannot currently explain in depth how both missense variants affect the function of FILIP1. Pro1133 is located in a part of FILIP1 (KVTSTITITPVTTSSTR) that is highly conserved between species and also between FILIP1 and the homologous protein FILIP1L. Since this variant is localized in a region of FILIP1 that binds filamins, it is plausible that this interaction is disturbed, an assumption supported by the results of our immunofluorescence studies on fibroblasts showing irregular FLNc distribution but one that would require further confirmational studies such as immunoprecipitation. The second missense variant, p.[Arg386Cys], is predicted to partly disturb the coiled coil region of FILIP1, which we expected to have an effect on the efficiency of FILIP1 di- or oligomerization.[29] Our biochemical assays, however, indicated that at least *in vitro*, the p.[Arg386Cys] variant does not behave differently compared to the wild-type protein and formed dimers as well as tetramers. Nevertheless, *in silico* studies suggested a novel Van der Waals interaction between Cys386 and Met390 accompanied by a destabilizing effect on the protein.

The combination of the expression pattern of FILIP1, the diverse nature of the variants found in our patients and the identification of several binding partners important for normal muscle development and/or neuronal growth yield a good basis to explain the diverse symptoms observed in our patients. Moreover, one might speculate that in addition to the extent of disruption of functional interactions that may, as indicated by our immunofluorescence findings in *FILIP1*-mutant fibroblasts, affect FLNc and FLNa, the efficacy of compensatory mechanisms is crucial for clinical severity: FILIP1L is a highly homologous protein, and it cannot be excluded that a compensatory increase in different cell populations may mitigate the detrimental effect of loss of functional FILIP1. Along these lines it is important to note that FILIP1L is also highly expressed in cardiac muscle, a tissue spared by FILIP1opathy. Although one might speculate that the recessive inheritance pattern observed in our patients represents the most severe end of the clinical spectrum of FILIP1opathies, resulting in congenital onset, and that heterozygous parents or siblings may develop clinical signs with much later onset as is usually the case in myofibrillar myopathies, the absence of clinical findings in parents or grandparents as well as the reporting of non-disease-associated heterozygous variants in gnomAD argue against this assumption.

Conclusions

FILIP1 codes for filamin-A-interacting protein 1 (FILIP1), a structural protein which has been shown to play an essential role in the proper function of neurons and muscle cells. Here, we reported five patients with bi-allelic *FILIP1* variants causing the congenital manifestation of dysmorphic features and a spectrum of neurological symptoms including intellectual disability, speech impairment, brain malformations and myopathy. Muscle pathology is rather mild on the histological level and associated with altered Z-disc architecture and myofibrillar disintegration, presence of autophagic vacuoles and FLNc accumulation as shown by electron and immunofluorescence microscopy. *FILIP1*-mutant fibroblasts show decreased FLNc levels and exhibit dysregulation of several proteins crucial for functions along the neuromuscular axis and associated with neurological diseases that present with symptoms overlapping with those observed in *FILIP1* patients. Our study thus adds FILIP1 to the list of structural proteins responsible for a cluster of neuropaediatric symptoms with congenital onset. Our clinical comparisons revealed that symptoms such as facial dysmorphism, neurodevelopmental delay and myopathy are also partially and to varying degrees in agreement with clinical findings obtained in patients harbouring pathogenic variants in *FLNA* and *FLNC*, two genes encoding FILIP1 binding partners (Supplementary Table 4). The results of our studies show that FILIP1 is another protein associated with aggregate formation in protein aggregate myopathies including myofibrillar myopathies.

Data availability

The proteomic profiling data have been deposited in the ProteomeXchange Consortium via the PRIDE partner repository with the dataset identifier PXD036407 and a list of all regulated proteins can be found in the supplement (Supplementary Table 1).

Uncropped gels and blots are presented as Supplementary material (see the 'Results' section).

Acknowledgements

The authors are grateful to the participants and their families, without whose support this work would not have been possible, and to T. Rollar, C. Mirschkorsch, Dr C. Preusse, Dr T. B. Haack as well as to Dr M. Sturm for excellent assistance. A sincere thank you to Dr R. Thompson for her diligent proofreading of this paper.

Funding

This work was supported by a grant of the French Muscular Dystrophy Association (AFM-Téléthon; #21644) to A.R. Parts of this study were financed in the framework of the NME-GPS project by the European Regional Development Fund (ERDF). Exome sequencing and development of bioinformatics pipelines for exome analysis in Patient 4 was supported by funds from the Universitätsklinikum Essen (allocated to C.D.). This study was moreover supported by the 'Ministerium für Kultur und Wissenschaft des Landes Nordrhein-Westfalen', the 'Regierenden Bürgermeister von Berlin - Senatskanzlei Wissenschaft und Forschung', and the 'Bundesministerium für Bildung und Forschung'. H.L. receives support from the Canadian Institutes of Health Research (Foundation Grant FDN-167281, Team Grant ERT-174211), the Canadian Institutes of Health Research and Muscular Dystrophy Canada (Network Catalyst Grant for NMD4C NG2-170044), the Canada Foundation for Innovation (CFI-JELF 38412), and the Canada Research Chairs program (Canada Research Chair in Neuromuscular Genomics and Health, 950-232279). Parts of the study were supported by the Solve-RD project which received funding from the European Union's Horizon 2020 research and innovation programme under Grant Agreement No. 779257. D.O.F. was supported by the German Research Foundation (FU 339/7-2 and FU 339/13-1). D.O.F. kindly thanks the Core Facility AIMBIOS, University of Bonn, for help with imaging. Data were analysed using the RD-Connect Genome-Phenome Analysis Platform, which received funding from EU projects RD-Connect, Solve-RD and EJP-RD (Grant Numbers FP7 305444, H2020 779257, H2020 825575).

Competing interests

The authors report no competing interests.

Supplementary material

Supplementary material is available at *Brain* online.

References

1. Benarroch L, Bonne G, Rivier F, Hamroun D. The 2021 version of the gene table of neuromuscular disorders (nuclear genome). *Neuromuscul Disord*. 2020;30:1008-1048.
2. Nagano T, Morikubo S, Sato M. Filamin A and FILIP (filamin A-interacting protein) regulate cell polarity and motility in neocortical subventricular and intermediate zones during radial migration. *J Neurosci*. 2004;24:9648-9657.
3. Meliota G, Vairo U, Ficarella R, Milella L, Faienza MF, D'Amato G. Cardiovascular, brain, and lung involvement in a newborn with a novel FLNA mutation: a case report and literature review. *Adv Neonatal Care*. 2022;22:125-131.
4. Gad AKB, Nehru V, Ruusala A, Aspenström P. Rhod regulates cytoskeletal dynamics via the actin nucleation-promoting factor WASp homologue associated with actin Golgi membranes and microtubules. *Mol Biol Cell*. 2012;23:4807-4819.
5. Militello G, Hosen MR, Ponomareva Y, *et al*. A novel long noncoding RNA myolinc regulates myogenesis through TDP-43 and filip1. *J Mol Cell Biol*. 2018;10:102-117.
6. Reimann L, Schwäble AN, Fricke AL, *et al*. Phosphoproteomics identifies dual-site phosphorylation in an extended basophilic motif regulating FILIP1-mediated degradation of filamin-C. *Communications biology*. 2020;3:253.
7. Kölbel H, Roos A, van Der Ven PF, *et al*. First clinical and myopathological description of a myofibrillar myopathy with congenital onset and homozygous mutation in *FLNC*. *Hum Mutat*. 2020;41:1600-1614.
8. Verdonschot JAJ, Vanhoutte EK, Claes GRF, *et al*. A mutation update for the *FLNC* gene in myopathies and cardiomyopathies. *Hum Mutat*. 2020;41:1091-1111.
9. Köster J, Dijkstra LJ, Marschall T, Schönhuth A. Varlociraptor: enhancing sensitivity and controlling false discovery rate in somatic indel discovery. *Genome Biol*. 2020;21:98.
10. Falb RJ, Muller AJ, Klein W, *et al*. Bi-allelic loss-of-function variants in *KIF21A* cause severe fetal akinesia with arthrogryposis multiplex. *J Med Genet*. 2023;60:48-56.
11. Kircher M, Witten DM, Jain P, O'Roak BJ, Cooper GM, Shendure J. A general framework for estimating the relative pathogenicity of human genetic variants. *Nat Genet*. 2014;46:310-315.

12. Wright CF, FitzPatrick DR, Ware JS, Rehm HL, Firth HV. Importance of adopting standardized MANE transcripts in clinical reporting. *Genet Med*. 2023;25:100331.
13. Katona I, Weis J, Hanisch F. Glycogenosome accumulation in the arrector pili muscle in Pompe disease. *Orphanet J Rare Dis*. 2014;9:17.
14. van der Ven PF, Obermann WM, Lemke B, Gautel M, Weber K, Fürst DO. Characterization of muscle filamin isoforms suggests a possible role of gamma-filamin/ABP-L in sarcomeric Z-disc formation. *Cell Motil Cytoskeleton*. 2000;45:149-162.
15. Kebir S, Orfanos Z, Schuld J, *et al*. Sarcomeric lesions and remodeling proximal to intercalated disks in overload-induced cardiac hypertrophy. *Exp Cell Res*. 2016;348:95-105.
16. van der Ven PF, Ehler E, Vakeel P, *et al*. Unusual splicing events result in distinct Xin isoforms that associate differentially with filamin c and mena/VASP. *Exp Cell Res*. 2006;312:2154-2167.
17. Obermann WM, Gautel M, Weber K, Fürst DO. Molecular structure of the sarcomeric M band: mapping of titin and myosin binding domains in myomesin and the identification of a potential regulatory phosphorylation site in myomesin. *EMBO J*. 1997; 16:211-220.
18. Guettsches AK, Meyer N, Zahedi RP, *et al*. FYCO1 increase and effect of arimoclomol-treatment in human VCP-pathology. *Biomedicines*. 2022;10:2443.
19. Hentschel A, Czech A, Münchberg U, *et al*. Protein signature of human skin fibroblasts allows the study of the molecular etiology of rare neurological diseases. *Orphanet J Rare Dis*. 2021; 16:73.
20. Arganda-Carreras I, Fernandez-Gonzalez R, Munoz-Barrutia A, Ortiz-De-Solorzano C. 3D Reconstruction of histological sections: application to mammary gland tissue. *Microsc Res Tech*. 2010;73:1019-1029.
21. Gungor S, Oktay Y, Hiz S, *et al*. Autosomal recessive variants in TUBGCP2 alter the gamma-tubulin ring complex leading to neurodevelopmental disease. i*Science*. 2021;24:101948.
22. Nagano T, Yoneda T, Hatanaka Y, Kubota C, Murakami F, Sato M. Filamin A-interacting protein (FILIP) regulates cortical cell migration out of the ventricular zone. *Nat Cell Biol*. 2002;4: 495-501.
23. Jumper J, Evans R, Pritzel A, *et al*. Highly accurate protein structure prediction with AlphaFold. *Nature*. 2021;596:583-589.
24. Chen Y, Lu H, Zhang N, Zhu Z, Wang S, Li M. PremPS: predicting the impact of missense mutations on protein stability. *PLoS Comput Biol*. 2020;16:e1008543.
25. Maerkens A, Olivé M, Schreiner A, *et al*. New insights into the protein aggregation pathology in myotilinopathy by combined proteomic and immunolocalization analyses. *Acta Neuropathol Commun*. 2016;4:8.
26. Kley RA, Maerkens A, Leber Y, *et al*. A combined laser microdissection and mass spectrometry approach reveals new disease relevant proteins accumulating in aggregates of filaminopathy patients. *Mol Cell Proteomics*. 2013;12:215-227.
27. Yagi H, Nagano T, Xie MJ, *et al*. Filamin A-interacting protein (FILIP) is a region-specific modulator of myosin 2b and controls spine morphology and NMDA receptor accumulation. *Sci Rep*. 2014;4:6353.
28. Jiang K, Toedt G, Montenegro Gouveia S, *et al*. A proteome-wide screen for mammalian SxIP motif-containing microtubule plus-end tracking proteins. *Curr Biol*. 2012;22:1800-1807.
29. Yagi H, Takabayashi T, Xie MJ, Kuroda K, Sato M. Subcellular distribution of non-muscle myosin IIb is controlled by FILIP through Hsc70. *PloS one*. 2017;12:e0172257.
30. Furst DO, Goldfarb LG, Kley RA, Vorgerd M, Olive M, van der Ven PF. Filamin C-related myopathies: pathology and mechanisms. *Acta Neuropathol*. 2013;125:33-46.
31. Sato M, Nagano T. Involvement of filamin A and filamin A-interacting protein (FILIP) in controlling the start and cell shape of radially migrating cortical neurons. *Anat Sci Int*. 2005;80:19-29.
32. Mattila PK, Lappalainen P. Filopodia: molecular architecture and cellular functions. *Nat Rev Mol Cell Biol*. 2008;9:446-454.
33. Pchitskaya E, Rakovskaya A, Chigray M, Bezprozvanny I. Cytoskeleton protein EB3 contributes to dendritic spines enlargement and enhances their resilience to toxic effects of beta-amyloid. *Int J Mol Sci*. 2022;23:2274.
34. Ciryam P, Antalek M, Cid F, *et al*. A metastable subproteome underlies inclusion formation in muscle proteinopathies. *Acta Neuropathol Commun*. 2019;7:197.
35. Becker K, Di DN, Holder-Espinasse M, *et al*. De novo microdeletions of chromosome 6q14.1-q14.3 and 6q12.1-q14.1 in two patients with intellectual disability - further delineation of the 6q14 microdeletion syndrome and review of the literature. *Eur J Med Genet*. 2012;55:490-497.
36. Gulsuner S, Walsh T, Watts AC, *et al*. Spatial and temporal mapping of de novo mutations in schizophrenia to a fetal prefrontal cortical network. *Cell*. 2013;154:518-529.
37. Kley RA, Leber Y, Schrank B, *et al*. FLNC-Associated Myofibrillar Myopathy: new clinical, functional, and proteomic data. *Neurol Genet*. 2021;7:e590.
38. Ailenberg M, Silverman M. Cytochalasin D disruption of actin filaments in 3T3 cells produces an anti-apoptotic response by activating gelatinase A extracellularly and initiating intracellular survival signals. *Biochim Biophys Acta*. 2003;1593(2-3):249-258.